

Mechanical characterization and cleaning of CVD single-layer h-BN resonators

Cartamil-Bueno, Santiago J.; Cavalieri, Matteo; Wang, Ruizhi; Hourri, Samer; Hofmann, Stephan; van der Zant, Herre S.J.

DOI

[10.1038/s41699-017-0020-8](https://doi.org/10.1038/s41699-017-0020-8)

Publication date

2017

Document Version

Final published version

Published in

npj 2D Materials and Applications

Citation (APA)

Cartamil-Bueno, S. J., Cavalieri, M., Wang, R., Hourri, S., Hofmann, S., & van der Zant, H. S. J. (2017). Mechanical characterization and cleaning of CVD single-layer h-BN resonators. *npj 2D Materials and Applications*, 1(1), Article 16. <https://doi.org/10.1038/s41699-017-0020-8>

Important note

To cite this publication, please use the final published version (if applicable).
Please check the document version above.

Copyright

Other than for strictly personal use, it is not permitted to download, forward or distribute the text or part of it, without the consent of the author(s) and/or copyright holder(s), unless the work is under an open content license such as Creative Commons.

Takedown policy

Please contact us and provide details if you believe this document breaches copyrights.
We will remove access to the work immediately and investigate your claim.

ARTICLE OPEN

Mechanical characterization and cleaning of CVD single-layer h-BN resonators

Santiago J. Cartamil-Bueno¹, Matteo Cavalieri¹, Ruizhi Wang², Samer Hour¹, Stephan Hofmann² and Herre S. J. van der Zant¹

Hexagonal boron nitride is a 2D material whose single-layer allotrope has not been intensively studied despite being the substrate for graphene electronics. Its transparency and stronger interlayer adhesion with respect to graphene makes it difficult to work with, and few applications have been proposed. We have developed a transfer technique for this extra-adhesive material that does not require its visual localization, and fabricated mechanical resonators made out of chemical vapor-deposited single-layer hexagonal boron nitride. The suspended material was initially contaminated with polymer residues from the transfer, and the devices showed an unexpected tensioning when cooling them to 3 K. After cleaning in harsh environments with air at 450 °C and ozone, the temperature dependence changed with f_0Q products reaching 2×10^{10} Hz at room temperature. This work paves the way to the realization of highly sensitive mechanical systems based on hexagonal boron nitride, which could be used as an alternative material to SiN for optomechanics experiments at room temperature.

npj 2D Materials and Applications (2017)1:16; doi:10.1038/s41699-017-0020-8

INTRODUCTION

Hexagonal boron nitride (h-BN), also known as ‘white graphite’, is a layered material consisting of partially-ionic sp^2 -bonded boron and nitrogen atoms in a honeycomb arrangement with a van der Waals and slightly ionic AA’ stacking.^{1, 2} h-BN is a III-V indirect wide-bandgap semiconductor (5–6 eV)³ that has been proved to be the complement insulating material for graphene electronics.⁴ The larger chemical and thermal stability of bulk h-BN compared to graphite have enabled applications in harsh environments such as deep ultraviolet photodetectors for space research^{5, 6} and high-performance lubricants.⁷

Among all the 2D materials, few studies on single-layer h-BN exist^{8, 9} despite the early attempts to exfoliate it¹⁰ and the well-developed synthesis techniques.^{11–17} The reason for its difficult exfoliation to a monolayer thickness is unclear, possibly being its AA’ stacking, its slightly-ionic bonds or flatness that causes adhesion between h-BN layers and other surfaces stronger than other 2D materials.^{18–21} Moreover, h-BN surfaces are hydrophilic in nature, but after being exposed to air they get covered by an hydrophobic layer of hydrocarbons as reported in h-BN nanotubes²² and graphene.²³ Understanding the adhesion, friction and other properties of single-layer h-BN can pave the way to promising applications, such as deep ultraviolet single photon emitters,^{24, 25} ultrathin piezotronics,^{26, 27} and to exploit its natural hyperbolic optical dispersion properties,²⁸ and proton conduction.²⁹

Fabrication of suspended h-BN devices has been limited to few-layers.^{30–32} Mechanical devices made out of 2D materials are often fabricated with a polymer-assisted transfer technique that requires a wet release of the suspended system,^{4, 8, 29} or a dry method that exploits the viscoelastic properties of polydimethylsiloxane (PDMS).^{33, 34} In the case of drum devices where the membrane seals a cavity of a few hundreds of nanometers in depth, a dry

transfer is more convenient as surface forces caused by liquid menisci upon drying tend to break the structure or push it to the bottom of the cavity resulting in collapsed devices.

In this work, we report the fabrication and characterization of mechanical resonators made out of chemical vapor-deposited (CVD) single-layer h-BN. The fabrication includes a novel transfer technique suitable for extra-adhesive 2D materials and highly efficient cleaning process for h-BN resonators. Due to the transfer process, the single-layer h-BN devices were covered with polymer contamination and showed an unexpected tensioning when cooling them to 3 K. After cleaning processes in harsh environments, the temperature dependence of their mechanical behavior changed, and their figure of merit (f_0Q product) improved by a factor of 30 up to 2×10^{10} Hz at room temperature.

RESULTS

Fabrication of h-BN microdrums

Figure 1a shows the fabrication process of suspended h-BN devices. A continuous layer of CVD h-BN is grown on iron foils and characterized by transmission electron microscopy (TEM) to be single layer as previously reported.¹⁷ Due to the stronger adhesion of h-BN to surfaces, it has to be transported from the growth substrate to the final substrate by using sacrificial layers. Poly (methyl methacrylate) (PMMA) is spin coated on top of the h-BN, and the stack is delaminated with the bubbling technique:³⁵ a voltage of 3 V is applied between the Fe/h-BN/PMMA stack (cathode) and a Pt wire (anode) of an electrochemical cell with 1 M NaOH (electrolyte). From scanning electron microscopy (SEM) images taken before the delamination, the grain size is estimated to be around 20 μm . The h-BN/PMMA stack is then transferred onto a piece of silicon covered with 300 nm of poly(vinyl alcohol)

¹Kavli Institute of Nanoscience, Delft University of Technology, Lorentzweg 1, Delft 2628CJ, The Netherlands and ²Department of Engineering, University of Cambridge, 9 JJ Thomson Avenue, Cambridge CB30FA, UK

Correspondence: Santiago J. Cartamil-Bueno (s.j.cartamilbueno@tudelft.nl)

Received: 26 October 2016 Revised: 24 May 2017 Accepted: 31 May 2017

Published online: 22 June 2017

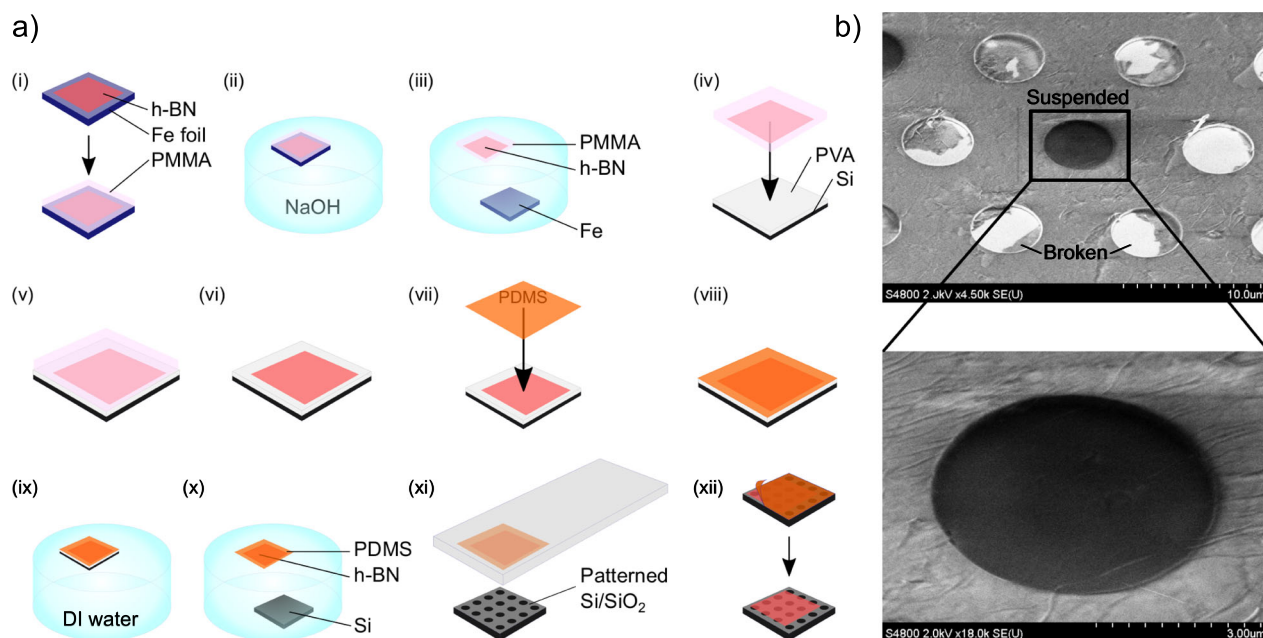


Fig. 1 CVD single-layer h-BN growth and dry transfer. **a** Large-area single-layer h-BN is grown by chemical vapor deposition (CVD) on Fe foils, and it is coated with PMMA (i). Then, the h-BN/PMMA stack is delaminated from the foil by means of bubbling¹⁷ (ii, iii). The h-BN is transferred to a Si/PVA substrate, and the PMMA is removed with acetone (iv–vi). PDMS is placed on the Si/PVA/h-BN (vii), and the structure is left floating on DI water (ix). When the Si substrate detaches from the layer stack (x), the h-BN/PDMS is picked and dried. From this point, the usual viscoelastic dry transfer technique³³ is used to transfer the CVD single-layer h-BN on patterned substrates (xi–xii). **b** Scanning electron microscope image of CVD single-layer h-BN covering circular cavities of 5 μm in diameter (*top panel*). Since h-BN is an insulator, electrons are trapped in the suspended material and appear with high contrast. A flat drum with a few wrinkles is shown in the *bottom panel*

(PVA), and the PMMA is removed by an acetone bath, resulting in a Si/PVA/h-BN structure.

Using this sandwiched structure, we developed a dry transfer technique that is a hybrid of the methods described in refs. 4, 33 especially designed for the transfer of CVD h-BN to make sealed cavities. Figure 1a (steps vi–xii) describes the dry transfer process. A piece of PDMS (GelPack × 8 PF film) is placed on top of the Si/PVA/h-BN, and the stack is left floating in deionized water. The water dissolves the PVA layer slowly until the h-BN/PDMS detaches from the silicon substrate which sinks. The floating h-BN/PDMS is picked up with tweezers and dried with nitrogen, and then placed on a clean microscope slide. From this point, we continue with the technique from reference:³³ the h-BN is dry transferred deterministically by using the viscoelastic properties of PDMS on top of the target substrate. A silicon substrate with 300 nm of thermally-grown SiO₂ is patterned via e-beam lithography and reactive ion etching to make circular cavities of different diameters on the oxide layer (fully etched through to the silicon). By using the developed transfer technique, we cover the cavities with CVD single-layer h-BN resulting in drums as shown in Fig. 1b. Some of these suspended membranes have small perforations, wrinkles and polymer contamination (see [Supplementary Information](#)).

Figure 2a shows the Raman spectrum with the characteristic peak at 1370 cm⁻¹,^{9, 36} which supports the TEM characterization on its single-layer nature. Moreover, the thickness and topographic flatness are measured with an atomic force microscope (AFM, Bruker Fastscan) in tapping mode (FastScan-A probe). As observed in Fig. 2b, the AFM indicates a thickness of 5 nm which is larger than that of a monolayer (0.44 nm), probably due to polymer contamination that disappears in some areas after cleaning processes as seen in Fig. 2c (more details in [Supplementary Information](#)).

Mechanical characterization

The static mechanical characterization of suspended CVD single-layer h-BN is performed by AFM nanoindentation. We use the Peak Force mode (ScanAsyst-Fluid probe) to deflect drums of 5 μm in diameter with a controlled force of 5 nN. Figure 3a shows the AFM image of the suspended drum from Fig. 1b with its corresponding force-deflection curve at its center. The tension and Young's modulus of the material are extracted by fitting the data for positive forces to the following equation valid for a circular structure under a central point load F :³⁷

$$F = \left[\frac{4\pi t^3 E}{3(1-\nu^2)R^2} + \pi N_0 \right] \delta + \frac{tE}{(1.05 - 0.15\nu - 0.16\nu^2)^3 R^2} \delta^3, \quad (1)$$

where N_0 , E and $\nu = 0.18$ ³⁸ are the pre-tension, Young's modulus and Poisson's ratio of the suspended material (chosen as an intermediate value in the range reported in literature), respectively; $t = 0.44$ nm is its thickness, R is the radius of the drum, and δ is the deflection induced by the AFM tip. The Young's modulus E is extracted by fitting the large-deformation data to the cubic term, although for small applied forces the accuracy is limited. The thickness-dependent term of the linear spring constant is negligible in these atomically-thin devices as the transfer of the material usually introduces stress that dominates the response at small deformations. This membrane behavior (e.g., tension dominated suspended structures) is found experimentally in the h-BN drums as shown below. The extracted tension and Young's modulus values are shown in Table 1 for five different drums, and they are expected to be influenced by the polymer in a second order of importance. Note the large Young's modulus of an undamaged drum (device 5), which is comparable to that of pristine graphene,³⁹ and the lower values obtained for the other perforated devices.

The mechanical properties are also measured indirectly from the drum dynamics with a laser interferometric technique in a

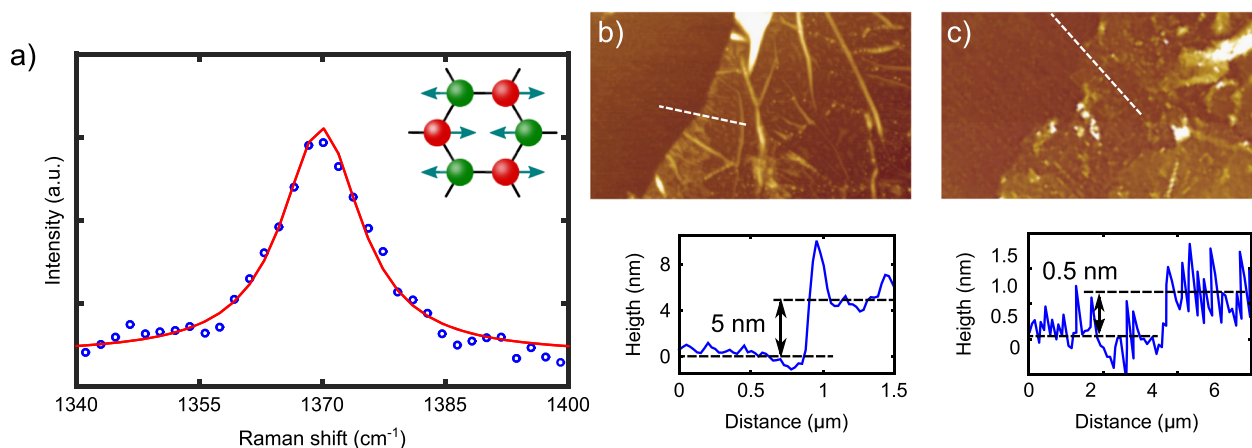


Fig. 2 Single-layer h-BN characterization. **a** Raman spectroscopy is used to determine the single-layer nature of the suspended material. As reported in ref. 9, we find a peak at 1370 cm^{-1} that corresponds to a monolayer h-BN. *Inset* Vibrational mode of a h-BN ring for that Raman frequency. **b** AFM height image of a h-BN material edge before cleaning. The obtained thickness (5 nm) is larger than that expected for single-layer (0.44 nm). The material is covered with polymer contamination that can be removed by oven annealing at $450\text{ }^{\circ}\text{C}$ in air and ozone as seen in **c**, where areas of 0.5 nm thick are found

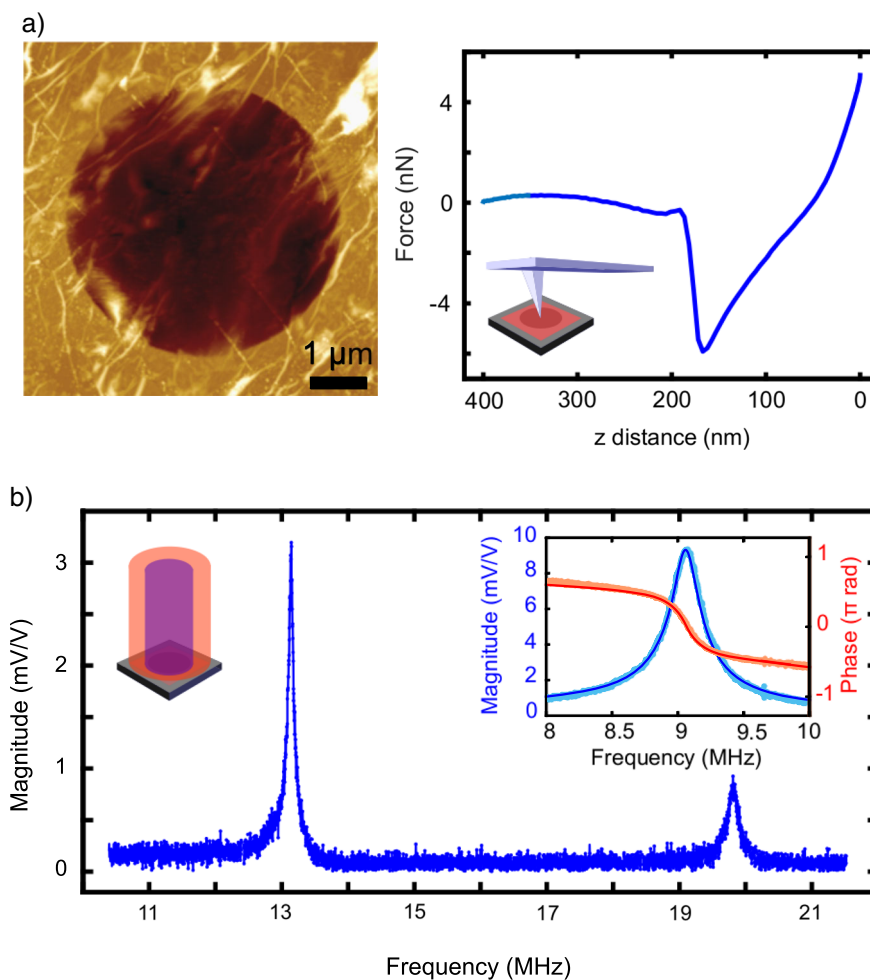


Fig. 3 Characterization of h-BN $5\text{ }\mu\text{m}$ in diameter drums. **a** AFM image of the h-BN drum showed in Fig. 1b. The CVD material shows wrinkles and sidewall adhesion as in CVD graphene (*left panel*). The force retraction curve in the center of the drum is obtained by AFM indentation in Peak Force mode. From the retraction curve we extract the tension and Young's modulus. **b** Mechanical frequency spectrum of the same drum at room temperature and $\sim 10^{-6}$ mbar when measured with the optical interferometric technique after cleaning. The second resonance peak appears around 1.5 times the fundamental frequency, indicating membrane behavior.³⁷ *Inset* Mechanical fundamental frequency and phase analysis of the same drum before cleaning. By fitting the frequency peak to the driven harmonic oscillator equation, we extract the tension values

cryo-station setup (Montana Instruments). A power-modulated diode laser ($\lambda = 405$ nm) photothermally actuates the drum, while a continuous-wave He-Ne laser ($\lambda = 633$ nm) allows the measurement of its resonance frequency f_0 .³⁴ Figure 3b displays the frequency spectrum of the same drum shown in Fig. 3a at a room temperature and pressure of $\sim 10^{-6}$ mbar, showing the fundamental mode around 13 MHz and the second (split) mode around 1.5 times the fundamental one. The factor of 1.5 indicates that the single-layer h-BN acts as a membrane in which pre-tension dominates over the bending rigidity.³⁷ The fundamental mode is given by:

$$f_0 = \frac{2.4}{2\pi R} \sqrt{\frac{N_0}{\rho t}}, \quad (2)$$

where $\rho = 2100$ kg/m³ is the mass density of the suspended material. By fitting the fundamental peak to the response function of a harmonic oscillator, we extract the resonance frequency that is used to calculate the tension from Eq. 2. The pre-tension values are shown in Table 2.

Temperature dependence of the resonance frequency

Figure 4 shows the temperature dependence of the fundamental frequency when cooling the device from 300 to 3 K. Equation 2 has to be modified to take into account the temperature-induced tensioning of the membrane due to the in-plane expansion coefficients of the 2D material and the underlying substrate dominated by the thermal expansion of the Si:

$$f_0(T) = \frac{2.4}{2\pi R} \sqrt{\frac{N_0 + N_{\text{adhesion}}(T)}{\rho t}}, \quad (3)$$

$$N_{\text{adhesion}}(T) = \begin{cases} Et \frac{\Delta T}{(1-\nu)} (\alpha_{\text{Si}} - \alpha_{\text{2D}}), & \alpha_{\text{Si}}(T) < \alpha_{\text{2D}}(T) \\ N_{\text{sidewall}}, & \alpha_{\text{Si}}(T) > \alpha_{\text{2D}}(T) \end{cases},$$

where α_{Si} and α_{2D} are the temperature-dependent expansion coefficient of silicon and the 2D material, respectively, in the basal plane; $\Delta T = T - 300$ K is the temperature difference from room

temperature. N_{sidewall} is a new tensioning mechanism that originates from the adhesion of the suspended 2D material to the sidewalls of the circular cavity, which happens when the membrane tries to expand laterally inside the cavity. This adhesion could balance out ($N_{\text{sidewall}} = 0$)⁴⁰ or increase the tension due to a biaxial in-plane strain ($N_{\text{sidewall}}(T) = Et\delta tL(T)/R^2 \propto \alpha_{\text{2D}}\Delta T$, where L is the change of adhered length on the sidewall).⁴¹ When cooling down the device made out of single-layer h-BN with negative in-plane thermal expansion coefficient ($\alpha_{\text{Si}}(T) > \alpha_{\text{h-BN}}(T)$), we would expect a constant or monotonic increase of f^2 , i.e., $f_0^2(T) - f_0^2(300\text{K}) \propto T$ with a zero or negative slope. The data, *red circles* in Fig. 4, show such a trend suggesting that $N_{\text{adhesion}} = N_{\text{sidewall}}$. However, another possible explanation for this could be residual resist remaining on top of the h-BN after transfer.

Impact of cleaning processes

To test this hypothesis, we clean the membranes by annealing the samples at 450 °C for 3.5 h in an air environment (78% N₂, 21% O₂), and in a further cleaning step using ultraviolet (UV)-induced ozone environment for 30 min. The oven annealing is expected to cause thermal and chemical degradations of polymers (boiling and evaporation of PVA, oxidation and gasification thermolysis of PMMA), and the UV ozone cleaning should produce photo-induced and chemical decomposition of polymers (photolysis of remaining PVA/PMMA and ozonolysis of PDMS) and decomposition of other organic matter with the UV ozone cleaning. Despite these cleaning processes in harsh environments, the h-BN remains suspended and the material becomes invisible under the optical microscope as expected from its low absorption of visible light,⁹ thus indicating that the contaminating polymer layer has been largely removed. After the treatments, the fundamental mode frequency at room temperature increased for all drums, although slightly. We also repeated the measurement as a function of temperature as shown in Fig. 4 by the *blue* (after oven annealing) and *black data points* (after ozone cleaning). More details about the temperature dependence of the mechanical properties of the h-BN drums can be found in [Supplementary Information](#) together with the complete dataset. The conclusion from the data is that when cooling a slight increase in the resonance frequency remains, although the effect is smaller than before annealing.

Table 1. Tension and Young's modulus values determined from AFM nanoindentation measurements for five different drums of 5 μm in diameter

Device	N_0 (10^{-3} N/m)	E (GPa)
1	21	102
2	25	199
3	21	186
4	38	81
5	48	936

Table 2. Fundamental frequency and tension of CVD single-layer h-BN drums at room temperature from the laser interferometric technique before and after cleaning in harsh environments

Device	Before cleaning		After oven annealing		After UV cleaning	
	f_0 (MHz)	N_0 (10^{-3} N/m)	f_0 (MHz)	N_0 (10^{-3} N/m)	f_0 (MHz)	N_0 (10^{-3} N/m)
1	8.5	2.7	14.8	8.6	9.1	3.3
2	9.9	3.7	13.5	7.2	14.2	7.9
3	10.0	3.8	17.8	12.5	19.9	15.6
4	10.4	4.1	9.9	3.9	17.0	11.4
5	9.1	3.1	13.2	6.8	20.3	16.3

DISCUSSION

References 8 and 16 report the mechanical characterization by AFM indentation of similar devices made out of CVD multilayer h-BN (1–2 and 5–15 nm in thickness, respectively). In those works, the material is placed on top of cavities with different transfer techniques that also introduce polymer contamination and wrinkles as we have observed in our devices by SEM and AFM. The Young's modulus reports (220–250 and 1160 GPa, respectively) are comparable to our measured values at room temperature, and in particular device 5 proves to have a stiffness close to the theoretical value of single-layer h-BN (885–995 GPa).

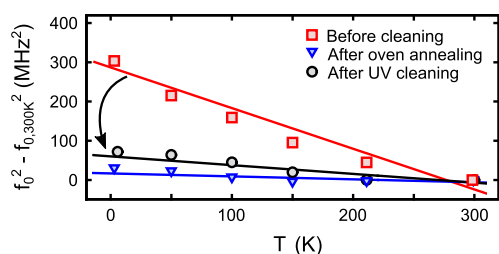


Fig. 4 Temperature dependence of the mechanical resonance frequency (fundamental mode) averaged for the h-BN drums before cleaning, after oven annealing, and after UV ozone cleaning. By cooling the drums from 300 K down to 3 K, the material is tensioned resulting in higher frequencies. Despite the expected negative in-plane thermal coefficient of h-BN, no compression is observed even after cleaning, hence suggesting that other tensioning mechanisms are present

In another work on graphene,⁴² the temperature-dependence of the Young's modulus was proven to be strongly influenced by the presence of wrinkles in the suspended membranes. More importantly, the previous works on h-BN present membranes that sag into the cavities due to the van der Waals forces between the material and the sidewalls. Considering that the 2D Young's modulus scales with the thickness, it is expected that single-layer h-BN shows larger sagging than previously reported (20–50 and 15 nm, in the mentioned works). AFM scans of our devices show sagging of 50–60 nm, thus supporting the monolayer nature of the material.

Bulk h-BN has a negative in-plane thermal expansion coefficient for temperatures higher than 75 K.⁴³ We assume that single-layer h-BN exhibits the same tendency as graphene with respect to graphite, i.e., that it has the same negative temperature dependence as in the bulk, but with a larger magnitude.⁴⁴ The observed tensioning must therefore originate from (a) an unexpected positive in-plane thermal expansion coefficient for h-BN as a single layer caused by the presence of polymer contamination even after cleaning,⁴⁵ (b) other tensioning mechanism such as the proposed sidewall adhesion or the presence of wrinkles, or (c) defect creation during UV ozone cleaning.

When comparing the tension values from the AFM and the laser interferometric studies as shown in Tables 1 and 2 (before cleaning), we observe a difference of one order of magnitude between the two. The indirect calculation of the tension from Eq. 2 includes the mass of the membrane as a parameter as opposed to the direct measurement, where the mass does not appear in Eq. 1. In fact, the thickness of the material measured by AFM before cleaning (5 nm, about 10 times that of single-layer h-BN) may explain the difference in values obtained from the AFM indentation and the laser interferometric techniques. The spread in values obtained with both techniques can also be justified with residues of inhomogeneous thickness and hence mass. In addition, the quality factors increased significantly with respect to the pre-cleaning values (see [Supplementary Information](#)), suggesting that the polymer residues play a significant role in damping the mechanical motion, probably due to their viscoelastic properties.

On the other hand, the increase of the fundamental frequencies at room temperature after cleaning (Table 2) indicates that either the oven annealing introduced larger pre-tensions (enhanced adhesion to the surface or the sidewall of the cavity) and/or a decrease in the mass (hence obtaining tensions more similar to those obtained from the AFM) according to Eq. 2. The mechanical quality factor of the resonators improved after each of the two cleaning steps (see [Supplementary Information](#)). This fact coupled to the disappearance of traces of polymer contaminants

and the on-average increase in the resonance frequency of the resonators suggests that polymer contamination is the main damping mechanism encountered in these resonators. It is unclear if there remains some polymer residue, although the tensioning trend when cooling has been reported in graphene and several transition metal dichalcogenide membranes.^{46–48} However, this trend should be explained differently for 2D materials with a negative expansion coefficient like h-BN or graphene,⁴⁹ and for that reason we propose an alternative tensioning effect caused by the sidewall adhesion, which should balance out or increase the tension when cooling certain 2D membranes, and explains our results and those on graphene drumheads. Other stronger cleaning routes for h-BN are available,^{50, 51} although not all of them might be compatible with suspended single-layer structures.

This study has presented the fabrication, mechanical characterization, and cleaning of CVD single-layer h-BN drumhead resonators. We have developed a transfer technique that allows the transfer of this extra-adhesive material from the growth substrate to a patterned SiO₂ surface with circular microcavities, resulting in suspended h-BN drums. The tension and Young's modulus of the material were characterized by performing AFM indentation on several devices, and the tension values are compared to those measured indirectly from the resonance frequency by means of laser interferometry. The temperature dependence of the dynamics of the drum is realized by cooling the devices to 3 K, and corroborates the assumption of having polymer residues covering the h-BN that dominates the tensioning of the devices. After cleaning in harsh environments, we observe a substantial improvement in the quality factor of the drums, and a change in their temperature-induced tensioning, which demonstrates cleaning of the suspended material. However, the temperature behavior suggests that some residues may still be present or that the structural mechanics model needs to be revisited for 2D materials, thus requiring further research. The strong adhesion of h-BN layers compared to other 2D materials could be exploited to make highly sensitive mechanical systems. Its electrical and optical properties are different than those from graphene, hence being a desirable material for applications where low-optical absorption or electrical insulation is required. Its nearly-zero extinction coefficient above 500 nm and good reflectivity could be used to make large f_0Q NEMS for optomechanics experiments. Moreover, it could be combined with other 2D materials to fabricate NEMS à la carte with new functionalities for transparent and flexible electronics.

METHODS

Raman spectroscopy

Raman spectroscopy on the h-BN material over Si/SiO₂ was carried out with a Renishaw in Via Raman microscope. Measurements with a laser light of 514 nm were performed on supported areas. The backscattered light was collected with a $\times 100$ objective (NA = 0.95) and recorded with a 1800 lines/mm grating, which gives a spectral resolution of ~ 1.75 cm⁻¹. The laser power was about 25 mW.

Atomic force microscopy

A Bruker Fastscan is used in tapping mode for imaging the topography and having a rough measurement of the material thickness (FastScan-A probe). For the mechanical characterization of suspended CVD single-layer h-BN, the AFM is calibrated and used in Peak Force mode for nanoindentation tests (ScanAsyst-Fluid probe, Peak Force setpoint of 5 nN).

Laser interferometry

The frequency response of the resonators is measured using a customized laser interferometer integrated into cryo-station (Montana Instruments). Two lasers are focused on the suspended drumheads with a microscope objective lens (Mitutoyo $\times 100$, NA = 0.75). The suspended material is

photothermally actuated with a modulated blue diode laser (Thorlabs LP405-SF10, $\lambda = 405$ nm) at a power of 260 μ W, while a second continuous-wave linearly-polarized Helium–Neon laser ($\lambda = 632.8$ nm) at 13 mW is used as optical probe for the detection.³⁴ The reflected red light is captured by a high speed photo-detector (NewFocus 1601) whose signal is crossed with the driving signal of the diode laser connected to a network analyzer (Rohde & Schwartz, ZVB4). The measurements are carried out in vacuum (10^{-6} mbar) for room temperature measurements, and higher vacuum when cooling.

Cleaning procedures

After fabrication and first measurements, the membranes are annealed at 450 °C for 3.5 h in an air environment (Lindberg/Blue tube furnace). After the immediate new round of measurements, we use a Novascan PSD-UVT decontamination system at room temperature to clean the samples using UV-induced ozone, which precedes another immediate round of measurements.

Data availability

The authors declare that the data supporting the findings of this study are available within the paper and its [supplementary information files](#).

ACKNOWLEDGEMENTS

The authors thank Joseph Scott Bunch, David Lloyd, Peter G. Steeneken and Barend J. Thijssse for discussions. The research leading to these results has received funding from the European Union's Horizon 2020 research and innovation programme under grant agreement No 649953 (Graphene Flagship). Ruizhi Wang acknowledges EPSRC Doctoral Training Award (EP/M506485/1). Stephan Hofmann acknowledges funding from EPSRC (Grant EP/K016636/1, GRAPHTEd) and ERC (Grant 279342, InsituNANO).

AUTHOR CONTRIBUTIONS

Experiments were designed by S.J.C.-B. and performed by S.J.C.-B. and M.C. Materials were designed and synthesized by St. H. and R.W. Data was analyzed by S.J.C.-B., M.C., and Sa. H., and all authors contributed to the discussion. S.J.C.-B. wrote the manuscript, with contributions from all authors.

ADDITIONAL INFORMATION

Supplementary Information accompanies the paper on the *npj 2D Materials and Applications* website (doi:10.1038/s41699-017-0020-8).

Competing interests: The authors declare that they have no competing financial interests.

Publisher's note: Springer Nature remains neutral with regard to jurisdictional claims in published maps and institutional affiliations.

REFERENCES

- Geick, R., Perry, C. & Rupprecht, G. Normal modes in hexagonal boron nitride. *Phys. Rev.* **146**, 543–547 (1966).
- Alem, N. et al. Atomically thin hexagonal boron nitride probed by ultrahigh-resolution transmission electron microscopy. *Phys. Rev. B* **80**, 1–7 (2009).
- Cassabois, G., Valvin, P. & Gil, B. Hexagonal boron nitride is an indirect bandgap semiconductor. *Nat. Photonics* **10**, 262–267 (2016).
- Dean, C. R. et al. Boron nitride substrates for high-quality graphene electronics. *Nat. Nanotechnol.* **5**, 722–6 (2010).
- Li, J. et al. Dielectric strength, optical absorption, and deep ultraviolet detectors of hexagonal boron nitride epilayers. *Appl. Phys. Lett.* **101**, 171112 (2012).
- Aldabahi, A. & Feng, P. Development of 2-D boron nitride nanosheets UV photoconductive detectors. *IEEE Trans. Electron Devices* **62**, 1885–1890 (2015).
- Kimura, Y., Wakabayashi, T., Okada, K., Wada, T. & Nishikawa, H. Boron nitride as a lubricant additive. *Wear* **232**, 199–206 (1999).
- Song, L. et al. Large scale growth and characterization of atomic hexagonal boron nitride layers. *Nano. Lett.* **10**, 3209–3215 (2010).
- Gorbachev, R. V. et al. Hunting for monolayer boron nitride: Optical and Raman signatures. *Small* **7**, 465–468 (2011).
- Pacile, D., Meyer, J. C., Girit, C. O. & Zettl, A. The two-dimensional phase of boron nitride: Few-atomic-layer sheets and suspended membranes. *Appl. Phys. Lett.* **92**, 133107 (2008).
- Nagashima, A., Tejima, N., Gamou, Y., Kawai, T. & Oshima, C. Electronic dispersion relations of monolayer hexagonal boron nitride formed on the Ni (111) surface. *Phys. Rev. B* **51**, 4606–4613 (1995).
- Rokuta, E. et al. Phonon dispersion of an epitaxial monolayer film of hexagonal boron nitride on Ni(111). *Phys. Rev. Lett.* **79**, 4609–4612 (1997).
- Kim, K. K. et al. Synthesis of monolayer hexagonal boron nitride on Cu foil using chemical vapor deposition. *Nano Lett.* **12**, 161–166 (2012).
- Kidambi, P. R. et al. In situ observations during chemical vapor deposition of hexagonal boron nitride on polycrystalline copper. *Chem. Mater.* **26**, 6380–6392 (2014).
- Lu, G. et al. Synthesis of large single-crystal hexagonal boron nitride grains on Cu-Ni alloy. *Nat. Commun.* **6**, 6160 (2015).
- Kim, S. M. et al. Synthesis of large-area multilayer hexagonal boron nitride for high material performance. *Nat. Commun.* **6**, 8662 (2015).
- Caneva, S. et al. Controlling catalyst bulk reservoir effects for monolayer hexagonal boron nitride CVD. *Nano. Lett.* **16**, 1250–1261 (2016).
- Martin, J. M., Le Mogne, T., Chassignette, C. & Gardos, M. N. Friction of hexagonal boron nitride in various environments. *Tribol. Trans.* **35**, 462–472 (1992).
- Nagashima, A. et al. Electron spectroscopic studies of monolayer hexagonal boron nitride physisorbed on metal surfaces. *Int. J. Mod. Phys. B* **10**, 3517–3537 (1996).
- Ooi, N., Rairkar, A., Lindsley, L. & Adams, J. B. Electronic structure and bonding in hexagonal boron nitride. *J. Phys. Condens. Matter* **18**, 97 (2006).
- Pizzocchero, F. et al. The hot pick-up technique for batch assembly of van der Waals heterostructures. *Nat. Commun.* **7**, 11894 (2016).
- Boinovich, L. B. et al. Origins of thermodynamically stable superhydrophobicity of boron nitride nanotubes coatings. *Langmuir* **28**, 1206–1216 (2012).
- Aria, A. I. et al. Time Evolution of the wettability of supported graphene under ambient air exposure. *J. Phys. Chem. C* **120**, 2215–2224 (2016).
- Tran, T. T., Bray, K., Ford, M. J., Toth, M. & Aharonovich, I. Quantum emission from hexagonal boron nitride monolayers. *Nat. Nanotechnol.* **11**, 37–41 (2015).
- Bourrellier, R. et al. Bright uv single photon emission at point defects in h-bn. *Nano. Lett.* **16**, 4317–4321 (2016).
- Duerloo, K. A. N., Ong, M. T. & Reed, E. J. Intrinsic piezoelectricity in two-dimensional materials. *J. Phys. Chem. Lett.* **3**, 2871–2876 (2012).
- Duerloo, K. A. N. & Reed, E. J. Flexural electromechanical coupling: A nanoscale emergent property of boron nitride bilayers. *Nano Lett.* **13**, 1681–1686 (2013).
- Castellanos-Gomez, A. Why all the fuss about 2D semiconductors? *Nat. Photonics* **10**, 202–204 (2016).
- Hu, S. et al. Proton transport through one-atom-thick crystals. *Nature* **516**, 227–230 (2014).
- Jo, I. et al. Thermal conductivity and phonon transport in suspended few-layer hexagonal boron nitride. *Nano Lett.* **13**, 550–554 (2013).
- Zhou, H. et al. High thermal conductivity of suspended few-layer hexagonal boron nitride sheets. *Nano Res.* **7**, 1232–1240 (2014).
- Zheng, X. Q., Lee, J. & Feng, P. X. L. Hexagonal boron nitride (h-BN) nano-mechanical resonators with temperature-dependent multimode operations. *2015 Transducers-2015 18th International Conference on Solid-State Sensors, Actuators and Microsystems (TRANSDUCERS)*, Vol. 2, 1393–1396 (IEEE, 2015).
- Castellanos-Gomez, A. et al. Deterministic transfer of two-dimensional materials by all-dry viscoelastic stamping. *2d Mater.* **1**, 011002 (2014).
- Cartamil-Bueno, S. J. et al. High-quality-factor tantalum oxide nanomechanical resonators by laser oxidation of TaSe₂. *Nano Res.* **8**, 2842–2849 (2015).
- Caneva, S. et al. Nucleation control for large, single crystalline domains of monolayer hexagonal boron nitride via Si-Doped Fe catalysts. *Nano. Lett.* **15**, 1867–1875 (2015).
- Cai, O. et al. Raman signature and phonon dispersion of atomically thin boron nitride. *Nanoscale* **9**, 3059–3067 (2017).
- Castellanos-gomez, A., Singh, V., Zant, H. S. J. V. D. & Steele, G. Mechanics of freely-suspended ultrathin layered materials. *Annalen der Physik* **527**, 27–44 (2015).
- Boldrin, L., Scarpa, F., Chowdhury, R. & Adhikari, S. Effective mechanical properties of hexagonal boron nitride nanosheets. *Nanotechnology* **22**, 505702 (2011).
- Lee, C., Wei, X., Kysar, J. W. & Hone, J. Measurement of the elastic properties and intrinsic strength of monolayer graphene. *Science* **321**, 385–388 (2008).
- Lu, Z. & Dunn, M. L. Van der Waals adhesion of graphene membranes. *J. Appl. Phys.* **107**, 044301 (2010).
- ASTM C1161-13. *Standard Test Method for Flexural Strength of Advanced Ceramics at Ambient Temperature*, 1–19 (ASTM International, 2013).
- Nicholl, R. J. T. et al. The effect of intrinsic crumpling on the mechanics of free-standing graphene. *Nat. Commun.* **6**, 8789 (2015).

43. Paszkowicz, W., Pelka, J., Knapp, M., Szyszko, T. & Podsiadlo, S. Lattice parameters and anisotropic thermal expansion of hexagonal boron nitride in the 10–297.5 K temperature range. *Appl. Phys. A Mater. Sci. Process.* **75**, 431–435 (2002).
44. Yoon, D., Son, Y. & Cheong, H. Negative Thermal Expansion Coefficient of Graphene Measured by Raman Spectroscopy. *Nano Lett.* **11**, 3227–3231 (2011).
45. Singh, V. et al. Probing thermal expansion of graphene and modal dispersion at low-temperature using graphene nanoelectromechanical systems resonators. *Nanotechnology* **21**, 165204 (2010).
46. Chen, C. et al. Performance of monolayer graphene nanomechanical resonators with electrical readout. *Nat. Nanotechnol.* **12**, 861–867 (2009).
47. Zande, A. Mvander et al. Large-scale arrays of Single-Layer Graphene Resonators. *Nano Lett.* **10**, 4869–4873 (2010).
48. Morell, N. et al. High quality factor mechanical resonators based on WSe₂ Monolayers. *Nano Lett.* **16**, 5102–5108 (2016).
49. Budrikis, Z. & Zapperi, S. Temperature-dependent adhesion of graphene suspended on a trench. *Nano Lett.* **16**, 387–391 (2016).
50. Garcia, A. G. F. et al. Effective cleaning of hexagonal boron nitride for graphene devices. *Nano Lett.* **12**, 4449–4454 (2012).
51. King, S. W., Nemanich, R. J. & Davis, R. F. Cleaning of pyrolytic hexagonal boron nitride surfaces. *Surf. Interface Anal.* **47**, 798–803 (2015).



Open Access This article is licensed under a Creative Commons Attribution 4.0 International License, which permits use, sharing, adaptation, distribution and reproduction in any medium or format, as long as you give appropriate credit to the original author(s) and the source, provide a link to the Creative Commons license, and indicate if changes were made. The images or other third party material in this article are included in the article's Creative Commons license, unless indicated otherwise in a credit line to the material. If material is not included in the article's Creative Commons license and your intended use is not permitted by statutory regulation or exceeds the permitted use, you will need to obtain permission directly from the copyright holder. To view a copy of this license, visit <http://creativecommons.org/licenses/by/4.0/>.

© The Author(s) 2017